

# Seismic analysis of the double-mode radial pulsator SX Phoenicis

J. Daszyńska-Daszkiewicz<sup>1</sup>★, A. A. Pamyatnykh<sup>2</sup>, P. Walczak<sup>1</sup>, W. Szewczuk<sup>1</sup>

<sup>1</sup>*Instytut Astronomiczny, Uniwersytet Wrocławski, Kopernika 11, 51-622 Wrocław, Poland*

<sup>2</sup>*Nicolaus Copernicus Astronomical Center, Bartycka 18, 00-716, Warsaw, Poland*

Accepted XXX. Received YYY; in original form ZZZ

## ABSTRACT

We present the results of complex seismic analysis of the prototype star SX Phoenicis. This analysis consists of a simultaneous fitting of the two radial-mode frequencies, the corresponding values of the bolometric flux amplitude (the parameter  $f$ ) and of the intrinsic mode amplitude  $\varepsilon$ . The effects of various parameters as well as the opacity data are examined. With each opacity table it is possible to find seismic models that reproduce the two observed frequencies with masses allowed by evolutionary models appropriate for the observed values of the effective temperature and luminosity. All seismic models are in the post-main sequence phase. The OPAL and OP seismic models are in hydrogen shell-burning phase and the OPLIB seismic model has just finished an overall contraction and starts to burn hydrogen in a shell. The OP and OPLIB models are less likely due to the requirement of high initial hydrogen abundance ( $X_0 = 0.75$ ) and too high metallicity ( $Z \approx 0.004$ ) as for a Population II star.

The fitting of the parameter  $f$ , whose empirical values are derived from multi-colour photometric observations, provides constraints on the efficiency of convective transport in the outer layers of the star and on the microturbulent velocity in the atmosphere. Our complex seismic analysis with each opacity data indicates low to moderately efficient convection in the star's envelope, described by the mixing length parameter of  $\alpha_{\text{MLT}} \in (0.0, 0.7)$ , and the microturbulent velocity in the atmosphere of about  $\xi_t \in (4, 8) \text{ km s}^{-1}$ .

**Key words:** stars: evolution – stars: oscillation – stars: Population II – stars: convection

## 1 INTRODUCTION

SX Phoenicis (HD 223065, SX Phe) is a star with the mean visual magnitude of  $V = 7.12$  mag and a A3V spectral type. The star belongs to Population II and was discovered to be variable by Eggen (1952a,b). Since then SX Phe became a prototype for the whole class of high-amplitude and, usually, metal-poor pulsators located inside the  $\delta$  Scuti instability strip. SX Phoenicis was a target of several studies based on photometric and spectroscopic observations. The analysis of photometric data revealed two frequencies and their combinations (e.g., by Coates et al. 1979; Rolland et al. 1991; Garrido & Rodriguez 1996) with the values  $\nu_1 = 18.1936 \text{ d}^{-1}$  and  $\nu_2 = 23.3794 \text{ d}^{-1}$  (Garrido & Rodriguez 1996). The frequency ratio indicates that SX Phe pulsates most probably in the two radial modes; the fundamental one and first overtone. These two periodicities were detected also in the radial velocity variations by Kim et al. (1993) with the amplitudes

of about  $18 \text{ km s}^{-1}$  for the dominant frequency and about  $4 \text{ km s}^{-1}$  for the secondary one. Quite surprisingly, the recent analysis of the high-precision photometry from the TESS satellite by Antoci et al. (2019) did not show any firm additional independent frequencies and, so far, confirmed the older results. The values of frequencies extracted from the TESS light curve of SX Phe are:  $\nu_1 = 18.193565(6) \text{ d}^{-1}$  and  $\nu_2 = 23.37928(2) \text{ d}^{-1}$ .

There is also some evidence that both pulsation periods change in a timescale of decades (Landes et al. 2007). Moreover, for the dominant pulsational period the effective temperature varies in a huge range from 7230 to 8210 K and the surface gravity from 4.25 to 3.86 dex (Rolland et al. 1991). The corresponding mean values are 7640 K and 3.89 (Kim et al. 1993). The recent determination of the effective temperature from spectroscopy amounts to  $T_{\text{eff}} = 7500(150) \text{ K}$  and the luminosity derived from the Gaia DR2 data is  $\log L/L_{\odot} = 0.844(9)$  (Antoci et al. 2019). The metallicity of SX Phe is typical for most stars of Population II. From photometric indexes, assuming a zero interstellar red-

★ E-mail: daszynska@astro.uni.wroc.pl

dening, [Rolland et al. \(1991\)](#) derived the value  $[m/H] = -1.0$  and [McNamara \(1997\)](#) the value  $[m/H] = -1.4$ . The most recent determination in [Antoci et al. \(2019\)](#) amounts to  $-1.00(15)$ . According to many determinations, the rotational velocity is low,  $V_{\text{rot}} = 18(2) \text{ km s}^{-1}$ , (e.g., [Rodríguez et al. 2000](#); [Antoci et al. 2019](#)).

There were several attempts to estimate a mass of SX Phe. [Vandenberg \(1985\)](#) obtained  $M = 1.2(1) M_{\odot}$  using evolutionary tracks for the helium abundance  $Y = 0.25$  and metallicity  $Z = 0.0017$ . Other determinations were based on the two radial-mode periods and/or pulsational equation. [Dziembowski & Kozłowski \(1974\)](#) indicated a small mass of about  $0.2 M_{\odot}$  whereas [Cox et al. \(1979\)](#) derived  $1.1 M_{\odot}$ . The values around one solar mass were obtained also by [Andreasen \(1983\)](#):  $M = 1.27 M_{\odot}$ , and [Eggen & Cox \(1989\)](#):  $M = 0.91 M_{\odot}$ . The seismic modelling with the early version of the OPAL opacity data ([Iglesias et al. 1992](#)) was performed by [Petersen & Christensen-Dalsgaard \(1996\)](#). These authors showed that the period ratio of the two radial modes is best reproduced by the model with parameters: a mass  $M = 1.0 M_{\odot}$ , metallicity  $Z = 0.001$ , initial hydrogen abundance  $X_0 = 0.70$  and age  $4.07 \text{ Gyr}$ . Recently, also initial results of our seismic modelling have been published in [Antoci et al. \(2019\)](#) and [Daszyńska-Daszkiewicz et al. \(2020\)](#).

The aim of this paper is to perform seismic modelling of SX Phe in a wide space of parameters and to study the effect of various opacity data. Besides, we try to reproduce the bolometric flux amplitude (the parameter  $f$ ) which is very sensitive to physical conditions in subphotospheric layers.

In Section 2, we present an independent mode identification from the Strömgren amplitudes and phases. Then, the results of fitting the two modes are given with detailed studies of the effects of various parameters as well as the opacity data. An attempt to reproduce also the parameter  $f$  of the two radial modes is shown in Section 3. The last section summarizes our results.

## 2 PULSATIONS OF SX PHOENICIS

Despite several efforts to find more periodic signals in the highly-asymmetric light curve of SX Phe, it seems that mainly the two frequencies are responsible for the variability of the star. From the Fourier analysis of the TESS light curve, it appeared that down to an amplitude of 1 ppt, there are two main frequencies with the values  $\nu_1 = 18.193565(6) \text{ d}^{-1}$  and  $\nu_2 = 23.37928(2) \text{ d}^{-1}$  and the amplitudes of about 136 ppt and 33 ppt, respectively ([Antoci et al. 2019](#)). Other five independent frequencies with very low amplitudes, but above 1 ppt, are in the frequency range  $(17, 50) \text{ d}^{-1}$ . Besides, many combinations and harmonic frequencies, up to the 7th one, were identified. In total, 27 frequency peaks were extracted from the TESS light curve.

As noticed in many earlier papers, the frequency ratio  $\nu_1/\nu_2 = 0.778192(6)$  indicates that these two frequencies can correspond to the consecutive radial modes: fundamental and first overtone. Here, we add for the first time an independent mode identification based on the photometric amplitudes and phases.

### 2.1 Independent mode identification

In the framework of linear theory of stellar pulsations, assuming the zero-rotation approach, the complex amplitude of a given mode in passband  $\lambda$  is given by (e.g., [Daszyńska-Daszkiewicz et al. \(2002\)](#)):

$$\mathcal{A}_{\lambda}(i) = -1.086 \varepsilon Y_{\ell}^m(i, 0) b_{\ell}^{\lambda} (D_{1,\ell}^{\lambda} f + D_{2,\ell} + D_{3,\ell}^{\lambda}) \quad (1)$$

where

$$D_{1,\ell}^{\lambda} = \frac{1}{4} \frac{\partial \log(\mathcal{F}_{\lambda} | b_{\ell}^{\lambda}|)}{\partial \log T_{\text{eff}}}, \quad (2a)$$

$$D_{2,\ell} = (2 + \ell)(1 - \ell), \quad (2b)$$

$$D_{3,\ell}^{\lambda} = - \left( 2 + \frac{\omega^2 R^3}{GM} \right) \frac{\partial \log(\mathcal{F}_{\lambda} | b_{\ell}^{\lambda}|)}{\partial \log g}. \quad (2c)$$

$\varepsilon$  is the intrinsic mode amplitude,  $i$  is the inclination angle and  $Y_{\ell}^m$  denotes the spherical harmonic with the degree  $\ell$  and the azimuthal order  $m$ . Symbols  $G, M, R, \omega$  have their usual meanings. The values of the amplitudes and phases themselves are given by  $A_{\lambda} = |\mathcal{A}_{\lambda}|$  and  $\varphi_{\lambda} = \arg(\mathcal{A}_{\lambda})$ , respectively.

As can be concluded from the above formula, the terms  $D_{1,\ell}^{\lambda}$ ,  $D_{2,\ell}$  and  $D_{3,\ell}^{\lambda}$  correspond to the effects of pulsational changes of temperature, geometry and pressure, respectively. The term  $b_{\ell}^{\lambda}$  is the integral of limb darkening weighted by the Legendre polynomial with the  $\ell$  degree. It describes the effect of disc averaging with increasing values of  $\ell$ . Derivatives of the monochromatic flux,  $\mathcal{F}_{\lambda}(T_{\text{eff}}, \log g)$ , as well as limb darkening and its derivatives are calculated from static atmosphere models. In general, their values depend on the metallicity  $[m/H]$  and microturbulence velocity  $\xi_t$ . Here, we rely on the Vienna atmosphere models (NEMO2003), which were computed with the modified versions of the ATLAS9 code ([Heiter et al. 2002](#)), in order to include turbulent convection treatment from [Canuto et al. \(1996\)](#). We added also our computations of model atmospheres for the microturbulent velocity  $\xi_t = 10 \text{ km s}^{-1}$ . Since we need only fluxes and specific intensities, we calculated these quantities using the atmosphere model from the original NEMO grid and the the SYNSPEC code with the microturbulent velocity set to  $\xi_t = 10 \text{ km s}^{-1}$  (e.g., [Hubeny & Lanz 2011, 2017](#)). Moreover, we derived the limb-darkening coefficients for the nonlinear formula of [Claret \(2000\)](#) for all values of  $\xi_t$ .

The parameter  $f$  describes the ratio of the bolometric flux perturbation to the radial displacement for a given pulsational mode:

$$\frac{\delta \mathcal{F}_{\text{bol}}}{\mathcal{F}_{\text{bol}}} = \text{Re}\{\varepsilon f Y_{\ell}^m(\theta, \varphi) e^{-i\omega t}\}. \quad (3)$$

The value of  $f$  is complex and can be obtained from non-adiabatic computations of stellar pulsations.

To identify pulsational modes of SX Phe, we followed the method of [Daszyńska-Daszkiewicz et al. \(2003\)](#). In this method, the mode degree  $\ell$ , the parameter  $f$  and the intrinsic mode amplitude, multiplied by the inclination-dependent factor,  $\varepsilon Y_{\ell}^m(i, 0)$  are determined simultaneously. It is achieved by fitting the theoretical values of the photometric amplitudes and phases to their observed counterparts. In this way, firstly, one avoids the uncertainties in the theoretical values of the parameter  $f$ , and secondly, valuable constraints on

**Table 1.** Amplitudes and phases in the TESS passbands (in units ppt) and the four Strömgren passbands (in units mag) for the two frequencies of SX Phoenixis. The frequencies are derived from the TESS light curve (Antoci et al. 2019).

	$A$ [ppt], [mag]	$\varphi$ [rad]
$\nu_1 = 18.193565 \text{ d}^{-1}$		
TESS	136.284(40)	
$u$	0.2046(6)	1.991(3)
$v$	0.2786(6)	1.864(2)
$b$	0.2511(6)	1.865(2)
$y$	0.2059(5)	1.851(2)
$\nu_2 = 23.379283 \text{ d}^{-1}$		
TESS	33.079(40) [ppt]	
$u$	0.0793(6)	3.768(7)
$v$	0.0993(6)	3.647(6)
$b$	0.0895(6)	3.653(6)
$y$	0.0742(5)	3.652(7)

the parameters of model and theory can be derived from a comparison of the theoretical and empirical values of  $f$ . In fact, we derive not the pure observational values  $f$  but the semi-empirical ones because one has to adopt some atmosphere models to compute the flux derivatives and limb darkening.

The goodness of the fit can be written as

$$\chi^2 = \frac{1}{2N - M} \sum_{i=1}^N \frac{|\mathcal{A}_{\lambda_i}^o - \mathcal{A}_{\lambda_i}^t|^2}{|\sigma_{\lambda_i}|^2}, \quad (4)$$

where  $N$  is the number of passbands  $\lambda_i$  and  $M$  is the number of parameters to be determined. The methods yields two complex parameters,  $\varepsilon$  and  $f$ , thus  $M = 4$ . The symbols  $\mathcal{A}^o$  and  $\mathcal{A}^t$  are complex observational and theoretical amplitudes, respectively, and  $\sigma_{\lambda_i}$  are their observational errors.

In the case of  $\delta$  Sct and SX Phe stars, the parameter  $f$  is very sensitive to the efficiency of convective transport in the outer layers. First successful applications of this method were demonstrated for  $\delta$  Sct pulsators by Daszyńska-Daszkiewicz et al. (2003, 2005a) and for  $\beta$  Cep pulsators by Daszyńska-Daszkiewicz et al. (2005b). In the case of B-type pulsator valuable constraints on stellar opacities were obtained (see Daszyńska-Daszkiewicz et al. 2017; Walczak et al. 2019). Moreover, the effect of atmosphere models was shown by Daszyńska-Daszkiewicz (2007).

The multicolour time-series photometry of SX Phe in the four Strömgren passbands was performed by Rolland et al. (1991). The values of amplitudes and phases in the Strömgren and TESS bands are given in Table 1. In Fig. 1, we show the values of the discriminant  $\chi^2$  as a function of the mode degree  $\ell$  for the dominant frequency (the left panel) and for the second frequency (the right panel). Four pairs ( $\log T_{\text{eff}}$ ,  $\log g$ ), spanning the ranges (3.855, 3.895) and (4.00, 4.15), respectively, were considered. The adopted atmospheric metallicity was  $[\text{m}/\text{H}] = -1.0$ . As one can see, the radial modes for both frequencies of SX Phe are clearly preferred.

**Table 2.** The effect of various parameters on the frequency ratio of the radial fundamental mode to the first overtone for models appropriated for SX Phoenixis.

The effect of $X$	
$X \nearrow \Rightarrow \frac{\nu_1}{\nu_2} \searrow$	
The effect of $Z$	
$Z \nearrow \Rightarrow \frac{\nu_1}{\nu_2} \searrow$	
The effect of $V_{\text{rot}}$	
$V_{\text{rot}} \nearrow \Rightarrow \frac{\nu_1}{\nu_2} \nearrow$	
The effect of $\alpha_{\text{ov}}$	
$\alpha_{\text{ov}} \nearrow \Rightarrow \frac{\nu_1}{\nu_2} \searrow$	
The effect of $\alpha_{\text{MLT}}$	
$\alpha_{\text{MLT}} \nearrow \Rightarrow \frac{\nu_1}{\nu_2} \approx \text{const}$	

## 2.2 Fitting the two radial-mode frequencies

Evolutionary computations were performed using the Warsaw-New Jersey code (e.g., Pamyatnykh et al. 1998; Pamyatnykh 1999). Three opacity tables were used: OPAL (Iglesias & Rogers 1996), OP (Seaton 1996, 2005) and OPLIB (Colgan et al. 2015, 2016). In each case, the lower temperature range, i.e., for  $\log T < 3.95$ , was supplemented with the data of Ferguson et al. (2005). The solar chemical mixture was adopted from Asplund et al. (2009). In all calculations the OPAL2005 equation of state was used (Rogers et al. 1996; Rogers & Nayfonov 2002). The Warsaw-New Jersey code takes into account the mean effect of the centrifugal force, assuming solid-body rotation and constant global angular momentum during evolution. The treatment of convection in the stellar envelope relies on the standard mixing-length theory.

Linear nonadiabatic oscillations were computed with the code of Dziembowski (1977a). The code takes into account the effects of rotation up to the second order. Convection flux is assumed to be constant during the pulsational cycle. This is so called the convective flux freezing approximation which is quite good if convection is not very efficient.

We search a wide space of parameters appropriate for SX Phe. As for the effective temperature we allowed for the whole range published in the literature, i.e.,  $\log T_{\text{eff}} \in (3.8483, 3.9325)$ . The value of luminosity  $\log L/L_{\odot} = 0.844(9)$  was adopted after Antoci et al. (2019) who determined it from the Gaia parallax using  $T_{\text{eff}}$  derived from the IRFM method. However, we allowed for the  $3\sigma$  error in  $\log L/L_{\odot}$ . The most recent determination of metallicity gives  $[\text{m}/\text{H}] = -1.00(15)$  (Antoci et al. 2019). Depending on the solar metallicity in model atmospheres used by the authors, the values of  $[\text{m}/\text{H}]$  translates into  $Z \in (0.0010, 0.0020)$  if the solar metallicity is  $Z_{\odot} = 0.014$  and into  $Z \in (0.0012, 0.0024)$  if  $Z_{\odot} = 0.017$ . The metallicity we searched encompasses much wider range, i.e.,  $Z \in (0.0008, 0.0040)$ .

We started the modelling with the OPAL opacity tables. For nonadiabatic convection in the outer layers we adopted the value of the mixing length parameter  $\alpha_{\text{MLT}} = 1.0$ . The

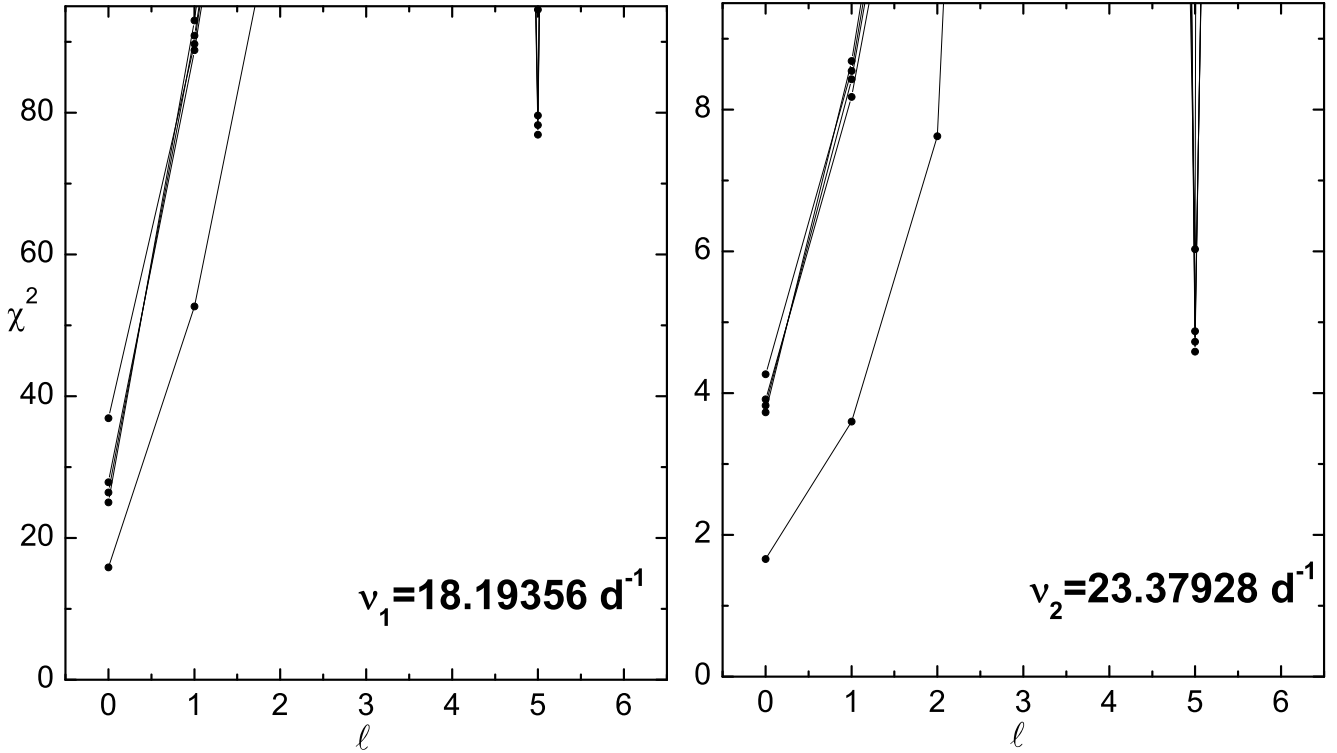


**Figure 1.** The values of  $\chi^2$  as a function of  $\ell$  for the two frequencies of SX Phe. NEMO model atmospheres were adopted with the metallicity  $[m/H] = -1.0$  and the microturbulent velocity  $\xi_t = 2 \text{ km s}^{-1}$ . The logarithmic values of the effective temperature  $\log T_{\text{eff}}$  and the surface gravity  $\log g$  are from the range (3.855, 3.895) and (4.00, 4.15), respectively. The left panel corresponds to the dominant frequency peak and the right one to the secondary peak.

value  $\alpha_{\text{MLT}} = 0.0$  means that convective transport does not take place in the stellar envelope. In the top panel of Fig. 2, we plot the frequency ratio of the radial fundamental mode to the first overtone as a function of a mass. All models reproduce exactly the dominant frequency  $\nu_1 = 18.193565 \text{ d}^{-1}$  corresponding to the radial fundamental mode. The theoretical value of the first overtone is in the range of about (23.2, 23.6)  $\text{d}^{-1}$ . Four cases are plotted to show the effect of the initial hydrogen abundance,  $X_0 = 0.67$  vs 0.70, metallicity,  $Z = 0.002$  vs 0.001, and the initial rotation  $V_{\text{rot},0} = 0$  vs  $15 \text{ km s}^{-1}$ . The observed value of the frequency ratio is marked as a horizontal line. The corresponding values of luminosity are depicted in the middle panel of Fig. 2. Because the considered value of  $V_{\text{rot}}$  is small, the luminosities for models with and without rotation overlap. The observed values of  $\log L/L_{\odot}$  are marked with the horizontal lines, allowing for the  $3\sigma$  error, i.e., from 0.817 to 0.871.

The first conclusion is that  $\nu_1/\nu_2(M)$  is not a monotonically decreasing function of a mass. As a consequence, there are two intersections with the line  $\nu_1/\nu_2 = 0.778192$ , corresponding to the observed value. The first intersection is for the mass of about  $M = 1.05 - 1.07 M_{\odot}$  and the second for  $M \approx 0.85 - 0.87 M_{\odot}$ . In all cases these low mass models have much too low luminosities. For lower metallicity  $Z = 0.001$  and  $X_0 = 0.67$  the first intersection is for much higher mass  $M \approx 1.31 M_{\odot}$  and luminosity  $\log L/L_{\odot} \approx 1.3$ , and the second one for much lower mass  $M < 0.8 M_{\odot}$  (not shown in the figure). Therefore we will not consider further this case.

As one can see from the top and middle panel of Fig. 2, only models computed with  $X_0 = 0.67$  and  $Z = 0.002$  with

masses of about  $M = 1.05 - 1.07 M_{\odot}$  are able to reproduce both the frequency ratio and luminosity. The model with  $M = 1.05 M_{\odot}$ , zero rotation and the parameters:  $\log T_{\text{eff}} = 3.8897$ ,  $\log L/L_{\odot} = 0.844$ ,  $R = 1.47 R_{\odot}$  has the frequency ratio  $\nu_1/\nu_2 = 0.77818$ . The age of this model is about 2.84 Gyr, thus it is much younger than the one found by Petersen & Christensen-Dalsgaard (1996). This model ideally reproduces both the observed frequencies and parameters, but the star must rotate.

Including the initial rotation of  $V_{\text{rot},0} = 15 \text{ km s}^{-1}$  for the same chemical composition we got the seismic model with the parameters:  $M = 1.073 M_{\odot}$ ,  $\log T_{\text{eff}} = 3.8969$ ,  $\log L/L_{\odot} = 0.878$ ,  $R = 1.48 R_{\odot}$  and  $\nu_1/\nu_2 = 0.77819$ . Thus, the model has the luminosity slightly above the  $3\sigma$  error of the observed value of  $\log L/L_{\odot}$ . From the top panel of Fig. 2, we can see that decreasing the rotational velocity will shift the line  $\nu_1/\nu_2(M)$  down. We found that the model with a mass  $M = 1.055 M_{\odot}$  and  $V_{\text{rot},0} = 10 \text{ km s}^{-1}$  would reproduce, both, the two frequencies and stellar parameters. The effective temperature, luminosity and radius of this model are  $\log T_{\text{eff}} = 3.8913$ ,  $\log L/L_{\odot} = 0.851$ ,  $R = 1.47 R_{\odot}$ , respectively. The frequency ratio of the two first radial modes is  $\nu_1/\nu_2 = 0.77819$ . The current rotation is  $V_{\text{rot}} = 9.8 \text{ km s}^{-1}$  and the age is 2.80 Gyr. The second intersection of the line  $\nu_1/\nu_2(M)$  with the observed frequency ratio occurs for the mass  $M = 0.838 M_{\odot}$  but the luminosity amounts only to about  $\log L/L_{\odot} = 0.46$ .

For hydrogen abundance  $X_0 = 0.70$ , metallicity  $Z = 0.002$  and zero-rotation, the model with the mass  $M \approx 1.02 M_{\odot}$  reproduces the two observed frequencies, but its



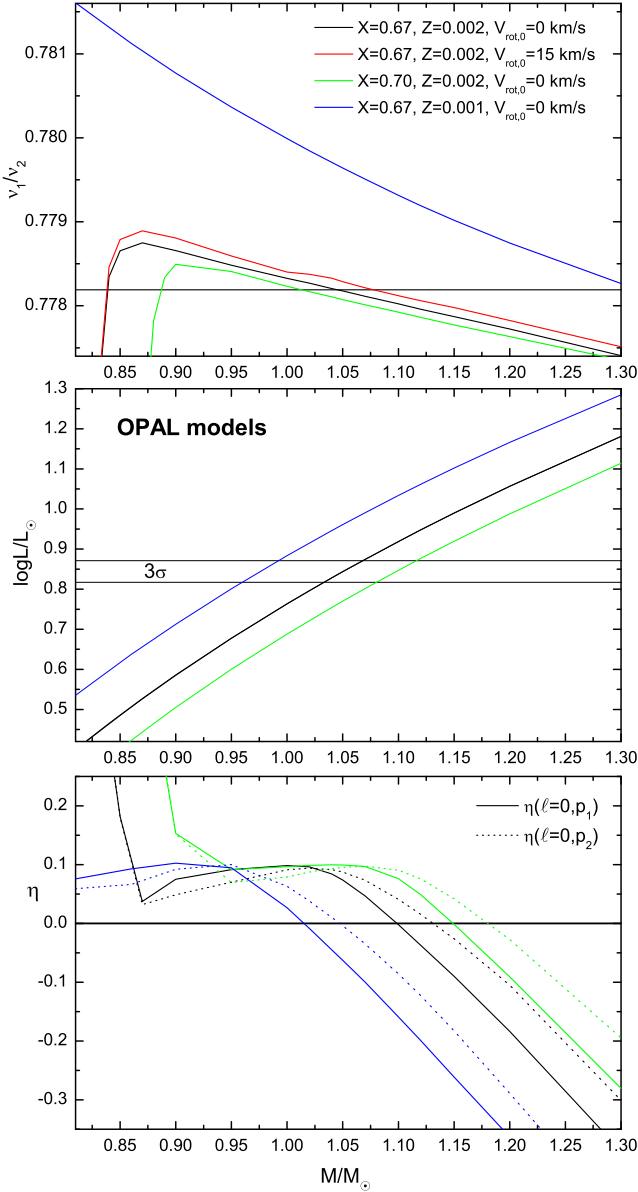


**Figure 2.** The top panel: the frequency ratio of the radial fundamental mode to the first overtone,  $\nu_1/\nu_2$ , as a function of a mass for models that fit the observed frequency  $\nu_1 = 18.19356 \text{ d}^{-1}$ . The models were computed with the OPAL opacity data. There is shown the effect of the initial hydrogen abundance ( $X_0 = 0.67$  vs  $0.70$ ), metallicity ( $Z = 0.002$  vs  $0.001$ ) and rotation ( $V_{\text{rot},0} = 0$  vs  $15 \text{ km s}^{-1}$ ). The middle panel: the corresponding values of luminosity. The luminosities for non-rotating and rotating models overlap. The horizontal lines indicate the observed range of luminosity, as determined from the Gaia parallax, allowing for the  $3\sigma$  error. The bottom panel: the corresponding values of the normalized instability parameter  $\eta$ . The solid lines correspond to the radial fundamental mode and the dashed ones to the first radial overtone. Modes with  $\eta > 0.0$  are excited.

luminosity is only  $\log L/L_{\odot} = 0.721$ . Increasing the initial rotational velocity to  $20 \text{ km s}^{-1}$ , we got the fit of the frequencies at the mass  $M = 1.082 M_{\odot}$ , effective temperature  $\log T_{\text{eff}} = 3.8814$  and the luminosity  $\log L/L_{\odot} = 0.819$ , which is at the edge of the  $3\sigma$  error. The model is  $3.07 \text{ Gyr}$  old. The rotation of this model is  $V_{\text{rot}} = 23.6 \text{ km s}^{-1}$  and its radius

$R = 1.48 R_{\odot}$ . One more best seismic model from our search, which reproduces both the observed frequencies and luminosity of SX Phe, has the following parameters:  $X_0 = 0.68$ ,  $Z = 0.002$ ,  $M = 1.06 M_{\odot}$ ,  $\log T_{\text{eff}} = 3.8867$ ,  $\log L/L_{\odot} = 0.834$ ,  $R = 1.47 R_{\odot}$ , and the current rotation  $V_{\text{rot}} = 14.4 \text{ km s}^{-1}$ . The age of this model is about  $2.92 \text{ Gyr}$ .

The five seismic models described above, with corresponding evolutionary tracks, are depicted with dots in Fig. 3. All of them are in the post-main sequence phase and burn hydrogen in the shell. There are shown also the OP and OPLIB seismic models with corresponding evolutionary tracks. They will be discussed in the next subsection.

The summary of the studied effects on the frequency ratio in the considered range of parameters is given in Table 2. The effect of overshooting from the convective core in the main sequence phase on the value of  $\nu_1/\nu_2$  for models with  $M \gtrsim 1.1 M_{\odot}$  is negligible and we did not include it in our computations. For example, the difference in  $\nu_1/\nu_2$  between the models with the overshooting parameter  $\alpha_{\text{ov}} = 0.0$  and  $\alpha_{\text{ov}} = 0.2$  is of the order of  $10^{-5}$ . Thus it is at the level of the numerical accuracy. Similarly, the value of the MLT parameter  $\alpha_{\text{MLT}}$ , describing the efficiency of nonadiabatic convection in the stellar envelope, has small effect on the frequency ratio. For example, the difference between the frequency ratio of models with masses around  $M = 1.05 M_{\odot}$  computed with  $\alpha_{\text{MLT}} = 0.0$  and  $\alpha_{\text{MLT}} = 1.0$  is of the order of  $10^{-5}$ .

It is quite probable that SX Phe itself is a blue straggler as many SX Phoenicis variables. Blue stragglers are presumably formed by the merger of two stars or by interactions in a binary system and, as a consequence, they may have enhanced helium abundance (e.g., McNamara 2011; Nemec et al. 2017).

Therefore, we consider models with a lower hydrogen (higher helium) abundance to be more preferred. These models rotate with the velocity of  $10 - 15 \text{ km s}^{-1}$ . The projected rotational velocity of SX Phe is  $V_{\text{rot}} \sin i = 18(2) \text{ km s}^{-1}$ , but most probably this value is overestimated because of a significant contribution of pulsation to the broadening of spectral lines. On the other hand, we cannot absolutely rule out the model with  $X_0 = 0.70$ ,  $Z = 0.002$ ,  $M = 1.082 M_{\odot}$ ,  $\log T_{\text{eff}} = 3.8814$ , and  $\log L/L_{\odot} = 0.819$  (if we accept the  $3\sigma$  error), rotating with the speed of  $23.6 \text{ km s}^{-1}$ .

To fully accept the seismic model, we have to ask about excitation of the two first radial modes. In the bottom panel of Fig. 2, we plotted the instability parameter  $\eta$  for models considered in the two upper panels. The parameter  $\eta$  is a normalized work integral and it is greater than zero for unstable (excited) pulsational modes. The solid lines represent the fundamental mode whereas the dashed ones the first overtone. The values of  $\eta$  for non-rotating and rotating models overlap. The horizontal line indicates  $\eta = 0.0$ . As one can see, in the case of  $X_0 = 0.67$ ,  $Z = 0.002$ , the models with masses  $M < 1.1 M_{\odot}$  have both radial modes unstable. As for other seismic models described above, all of them have also both the radial fundamental as well as first overtone modes unstable.

### 2.3 The effect of opacity data

In the next step, we performed the same seismic modelling using stellar opacities from the OP and OPLIB projects. The results are presented in the same way as for the OPAL mod-

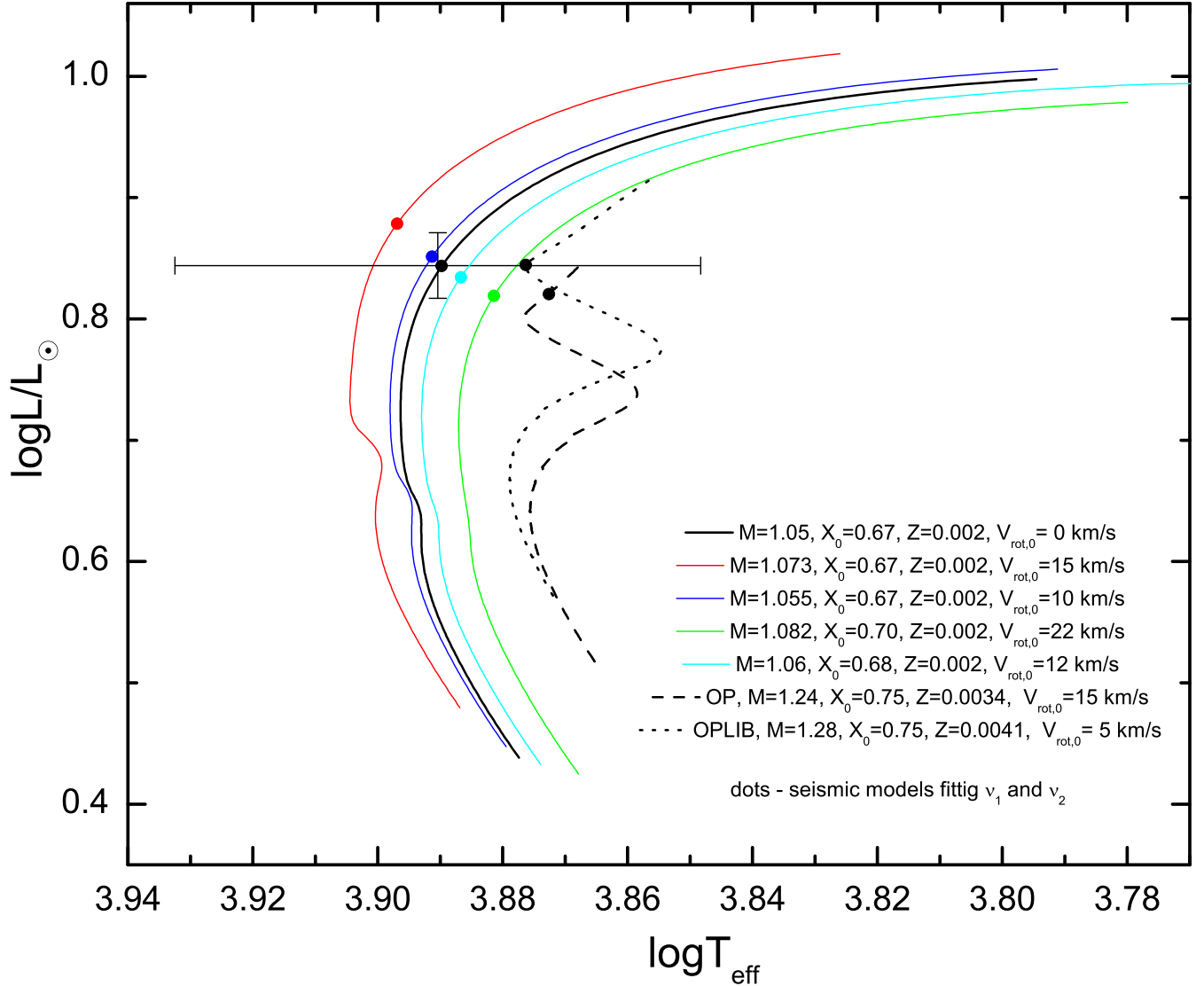


**Figure 3.** The HR diagram with the position of SX Phe and evolutionary tracks for various masses computed with the three opacity tables: OPAL, OP and OPLIB. The tracks computed adopting the OPAL data are depicted with the solid line whereas those computed adopting the OP and OPLIB data with dashed and dotted line, respectively. The models that reproduce the observed frequencies of the two radial modes are marked with dots. The  $3\sigma$  error was adopted for the the GAIA luminosity. For the effective temperature the whole range available in the literature was included. Masses in the legend are in solar units.

els in Figs. 4 and 5. As one can see from the top panels, now the values of the frequency ratio  $\nu_1/\nu_2$  of the models fitting the frequency  $\nu_1$  are much higher than the observed value both for the OP models (Fig. 4) and for the OPLIB models (Fig. 5). Thus, in the allowed range of mass and luminosity, there is no model with the frequency ratio  $\nu_1/\nu_2 = 0.77819$ . The intersections occurring at  $M = 0.81 - 0.87 M_{\odot}$  have luminosities  $\log L/L_{\odot} < 0.55$ . On the other hand, the models computed with the three sources of opacity data have very similar values of  $\log L/L_{\odot}$  (cf. middle panels of Figs. 2, 4, 5).

Considering what we have learned from seismic modelling of B-type stars (Daszyńska-Daszkiewicz et al. 2017; Walczak et al. 2019), this result is a bit surprising. In case of B-type pulsators with masses around  $8 - 12 M_{\odot}$ , seismic models computed with OPAL and OPLIB data had simi-

lar parameters. In the case of SX Phe, the OP and OPLIB seismic models are rather similar.

From the bottom panels of Figs. 4 and 5, we can see that the instability of the two radial modes are not affected by the opacity data. This means that in the region where pulsations are excited, i.e., around  $\log T \approx 4.66$ , the mean opacity and its derivatives must be very close. This is the case if we compare the values of  $\kappa(\log T \approx 4.66)$  and its temperature derivative for the model with parameters:  $X_0 = 0.67$ ,  $M = 1.05 M_{\odot}$ ,  $\log T_{\text{eff}} \approx 3.89$ ,  $\log L/L_{\odot} \approx 0.84$ ,  $V_{\text{rot}} = 0$ , computed with the three opacity data. The mean opacity for this model is shown in the left panel of Fig. 6. The corresponding values of the frequency ratio are:  $\nu_1/\nu_2(\text{OPAL}) = 0.77818$ ,  $\nu_1/\nu_2(\text{OP}) = 0.77992$ ,  $\nu_1/\nu_2(\text{OPLIB}) = 0.78080$ . Making the same comparison for other masses, we can say that in general, for a given mass which reproduces the frequency  $\nu_1$  we

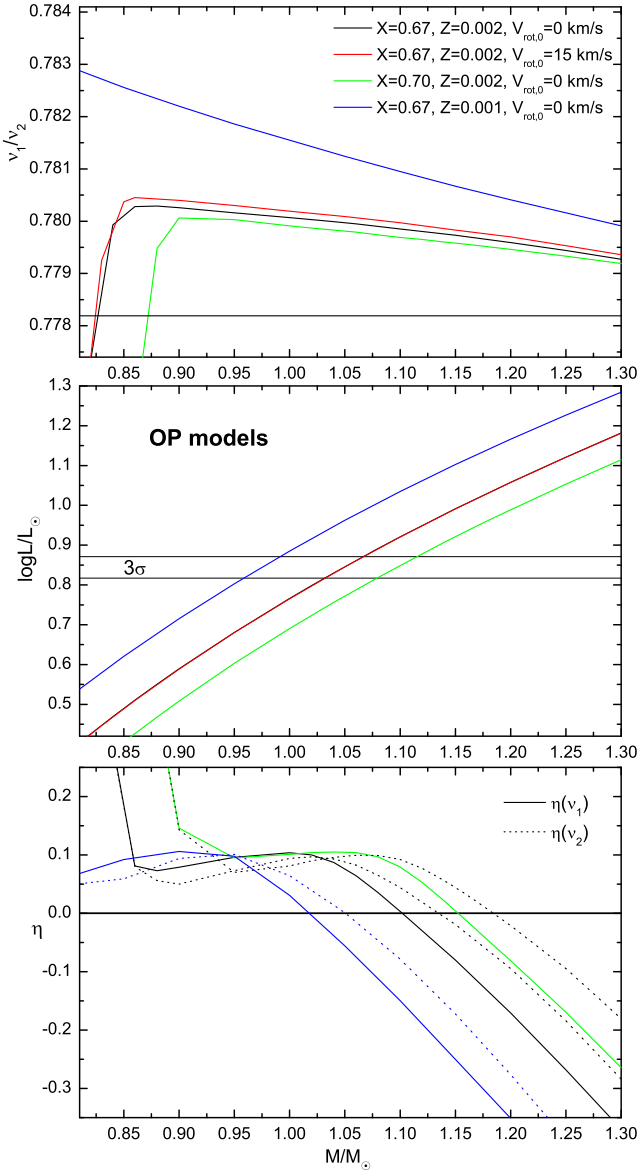


**Figure 4.** The same as in Fig. 2 but evolutionary models were computed adopting the OP opacities.

have:

$$\frac{\nu_1}{\nu_2}(\text{OPAL}) < \frac{\nu_1}{\nu_2}(\text{OP}) < \frac{\nu_1}{\nu_2}(\text{OPLIB}), \quad (5a)$$

thus

$$\nu_2(\text{OPAL}) > \nu_2(\text{OP}) > \nu_2(\text{OPLIB}). \quad (5b)$$

So, what is the reason for such differences in the frequency ratio?

From a very simple consideration for a homogeneous and adiabatic model, the frequency ratio of the radial fundamental mode to the first overtone can be expressed as a function of the adiabatic index  $\Gamma_1$  (e.g., [Kippenhahn et al. 2012](#)):

$$\left(\frac{\nu_1}{\nu_2}\right) = \frac{3\Gamma_1 - 4}{10\Gamma_1 - 4}, \quad (6)$$

where  $\Gamma_1 > 4/3$ . Although, the above formula is far from

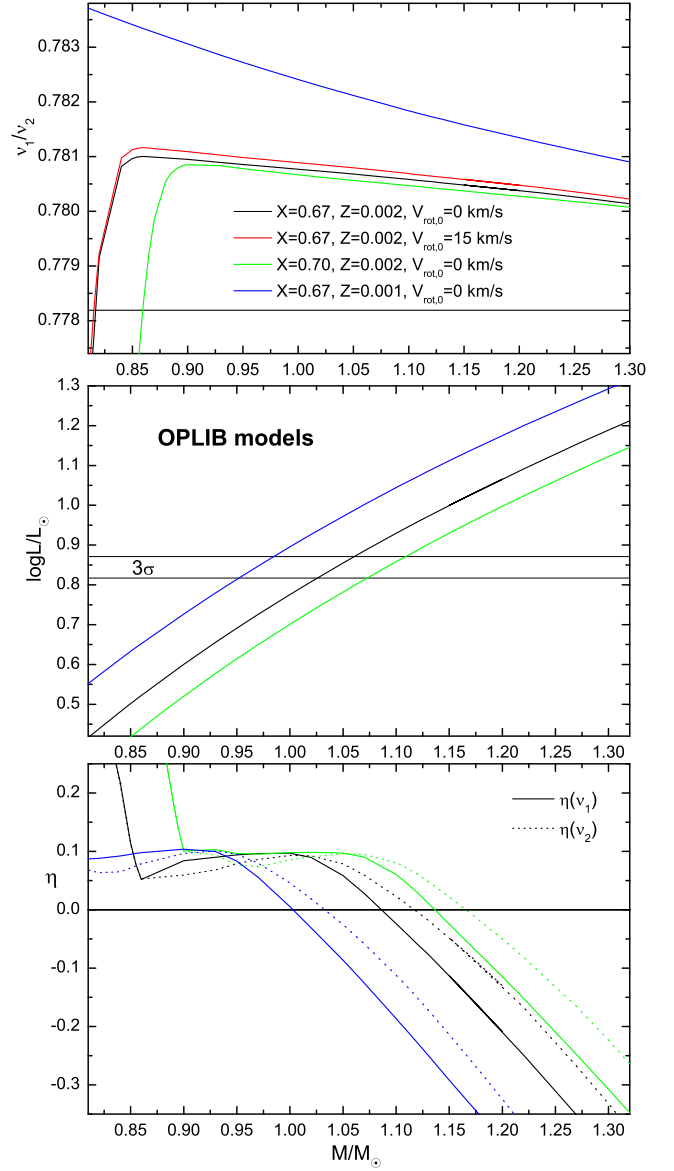


**Figure 5.** The same as in Fig. 2 but evolutionary models were computed adopting the OPLIB opacities.

strict, we can assume at least such proportionality. It implies that  $\nu_1/\nu_2$  is always a monotonically increasing function of  $\Gamma_1$ . Hence, we can infer that

$$\Gamma_1(\text{OPAL}) < \Gamma_1(\text{OP}) < \Gamma_1(\text{OPLIB}), \quad (7)$$

whereas for the radiative gradient  $\nabla_{\text{rad}} = (\partial \log T / \partial \log P)_{\text{rad}}$  we should have

$$\nabla_{\text{rad}}(\text{OPAL}) > \nabla_{\text{rad}}(\text{OP}) > \nabla_{\text{rad}}(\text{OPLIB}). \quad (8)$$

In the right panel of Fig. 6, we depicted the values of the radiative gradient for the OPAL, OP and OPLIB models. As one can see, the only difference is around  $\log T = 4.1$  where hydrogen ionization takes place. In other regions the values of  $\nabla_{\text{rad}}$  for models computed with the three opacity tables are equal up to the numerical accuracy. Indeed, the value of  $\nabla_{\text{rad}}(\log T = 4.1)$  for the OPAL model is the largest one. Thus, it seems that this region is responsible for the subtle differences in the frequency ratio.

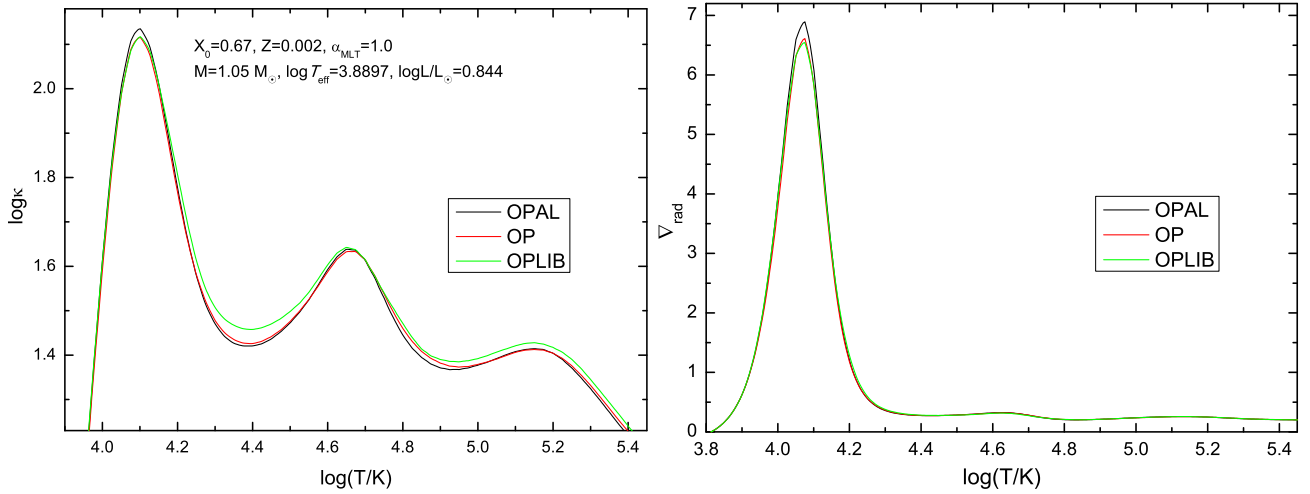


**Figure 6.** The left panel: the run of the mean Rosseland opacity inside the models computed for the same parameters but with different opacity data: OPAL, OP and OPLIB. The OPAL model reproduce the observed frequencies of the two radial modes of SX Phe as well as its effective temperature and GAIA luminosity. The model parameters are given in the legend. The right panel: the corresponding values of the radiative gradient  $\nabla_{\text{rad}}$ .

Of course, the natural question arises: is it possible to achieve the fit of the two frequencies and luminosity with OP and OPLIB opacities by changing, in a reasonable range, such parameters as mass, hydrogen abundance and metallicity?

The best fit with the OP data we obtained at the parameters:  $M = 1.24 M_{\odot}$ ,  $X_0 = 0.75$ ,  $Z = 0.0034$  and  $V_{\text{rot}} = 17 \text{ km s}^{-1}$ . The radius of this model is slightly larger comparing to the radii of the OPAL seismic models and amounts to  $R = 1.55 R_{\odot}$ . The logarithmic values of the effective temperature and luminosity are  $\log T_{\text{eff}} = 3.8725$  and  $\log L/L_{\odot} = 0.820$ , respectively. The age of this model is 2.62 Gyr. The position of the OP seismic model and the corresponding evolutionary track are shown on the HR diagram in Fig. 3. As one can see, the model is after an overall contraction, in the hydrogen shell-burning phase.

Similarly, using the OPLIB opacities, we had to increase significantly the initial hydrogen abundance and metallicity, up to  $X_0 = 0.75$ ,  $Z = 0.0041$ , respectively. The best OPLIB seismic model has the following parameters:  $M = 1.28 M_{\odot}$ ,  $R = 1.56 R_{\odot}$ ,  $\log T_{\text{eff}} = 3.8763$  and  $\log L/L_{\odot} = 0.845$  and rotates with the velocity of  $V_{\text{rot}} = 5.5 \text{ km s}^{-1}$ . Its age is 2.31 Gyr. The position of the OPLIB seismic model and the corresponding evolutionary track are also shown on the HR diagram in Fig. 3. The model has just finished the overall contraction phase.

As one can see, the OP and OPLIB models have rather high metallicity and initial hydrogen abundance. Therefore, we consider these seismic models less probable but we cannot exclude them with 100 per cent certainty.

### 3 CONSTRAINTS FROM THE PARAMETER $f$ AND INTRINSIC MODE AMPLITUDE $\varepsilon$

The method of mode identification described in Sect. 2.1, besides the mode degree  $\ell$ , provides the semi-empirical values of the two complex quantities: the parameter  $f$  and the mode amplitude  $\varepsilon$ . The parameter  $f$  is the amplitude of the

radiative flux variations at the level of the photosphere and  $\varepsilon$  give the relative radius variations. These two parameters are semi-empirical because their values depend on the model atmospheres, in particular, on the metallicity and microturbulent velocity  $\xi_t$ . However, for simplicity from now on, we will call the determined values of  $f$  and  $\varepsilon$  as "empirical". To this aim we used the time-series multicolour photometry of Rolland et al. (1991).

As we mentioned, in Sect. 2.1, the diagnostic potential of this method is huge as a comparison of the theoretical and empirical values of  $f$  yields valuable constraints on parameters of the model and theory. In particular, for AF-pulsators, one can expect valuable constraints on the efficiency of convective transport in the outer layers.

#### 3.1 The values of $f$ and $\varepsilon$ for models fitting the dominant frequency

In Fig. 7, we show a comparison of the empirical and theoretical values of  $f$  as a function of a mass. All models reproduce the frequency  $\nu_1 = 18.193565 \text{ d}^{-1}$  corresponding to the radial fundamental mode. The left panels correspond to the dominant mode frequency  $\nu_1 = 18.193565 \text{ d}^{-1}$  and the right panels to the second frequency  $\nu_2 \approx 23.38 \text{ d}^{-1}$ . In the top panels, a run of the real part of  $f$  is shown ( $f_R$ ) and in the bottom panels - the imaginary part of  $f$  ( $f_I$ ). Theoretical models were computed for the chemical composition  $X_0 = 0.67$ ,  $Z = 0.002$ , the OPAL opacities and the five values of the mixing length parameter  $\alpha_{\text{MLT}} = 0.0, 0.5, 1.0, 1.5, 2.0$ . The rotation was not taken into account. The empirical values of  $f$  were derived adopting Vienna model atmospheres for the metallicity  $[m/H] = -1.0$  and the four values of microturbulent velocity  $\xi_t = 2, 4, 8, 10 \text{ km s}^{-1}$ . The model which fits the two observed frequencies has a mass  $M = 1.05 - 1.06 M_{\odot}$  as was described in Sect. 2.2. As one can see from the left panels of Fig. 7, for the dominant frequency, also around this mass, we got the agreement between the theoretical and empirical values of  $f$ , simultaneous for the real and imaginary part, if the MLT parameter is below 1.0 and the mi-



roturbulent velocity is about  $8 \text{ km s}^{-1}$ . Worse agreement was obtained for the second frequency  $\nu_2$ . In that case, for  $M \approx 1.05M_\odot$ , one can adjust the real part  $f_R$  for  $\alpha_{\text{MLT}} < 0.5$  and  $\xi_t \approx 10 \text{ km s}^{-1}$ , whereas the imaginary part  $f_I$  for  $\alpha_{\text{MLT}} < 1.0$  and  $\xi_t \in (2, 4) \text{ km s}^{-1}$ . Nevertheless, the result is promising because the model reproduces two frequencies and the value of  $f$  for the dominant frequency, simultaneously. The best fit of the theoretical and observed amplitudes and phases is achieved for the model atmospheres with  $\xi_t = 4 \text{ km s}^{-1}$ . The results obtained for  $\xi_t = 10 \text{ km s}^{-1}$  are rather excluded because the goodness of the fit,  $\chi^2$ , is about 3–4 times worse than those obtained with  $\xi_t = 4 \text{ km s}^{-1}$ . We will come back to the detailed comparison of the empirical and theoretical values of  $f$  for seismic models in the next subsection.

Now let us discuss the values of the second parameter derived from the method, i.e., the intrinsic mode amplitude  $\varepsilon$ . In general, the method provides the value of  $\varepsilon Y_\ell^m(i, 0)$  but in the case of radial pulsation the absolute value of  $\varepsilon$  is obtained. The parameter  $\varepsilon$  defines the local radial displacement of the surface element, i.e.,

$$\frac{\delta r(R, \theta, \varphi)}{R} = \varepsilon Y_\ell^m(\theta, \varphi) e^{-i\omega t}, \quad (9)$$

where  $i$  is the imaginary unit. With the normalization of the spherical harmonics:

$$Y_\ell^m(\theta, \phi) = (-1)^{\frac{m+|m|}{2}} \sqrt{\frac{(2\ell+1)(\ell-|m|)!}{(\ell+|m|)!}} P_\ell^{|m|}(\cos \theta) e^{im\phi}, \quad (10)$$

$|\varepsilon|$  is the r.m.s. value of  $\delta r/R$  over the star surface. On the other hand the empirical value of  $\varepsilon$  can be estimated from the amplitude of radial velocity variations. For nonradial linear pulsation, the complex formula for this amplitude is as follows (Dziembowski 1977b)

$$A_{\text{Vrad}}(i) = i\varepsilon \omega R Y_\ell^m(i, 0) \left( u_\ell + \frac{GM}{R^3 \omega^2} v_\ell \right), \quad (11)$$

where  $u_\ell$  and  $v_\ell$  are another disc averaging factors expressed by the integrals from the limb darkening and Legendre polynomials.

For the radial pulsation,  $Y_\ell^m(i, 0) = 1$ , the factor  $v_\ell$  is equal zero and the value of  $u_\ell$  is 0.708 for the visual band, adopting model atmospheres with  $[m/H] = -1.0$  and  $T_{\text{eff}}$ ,  $\log g$  appropriate for SX Phe. Thus, we get for the absolute value of  $\varepsilon$

$$|\varepsilon(A_{\text{Vrad}}, R)| = \frac{A_{\text{Vrad}}}{0.708 \omega R}. \quad (12)$$

According to Kim et al. (1993), the observed amplitude of the radial velocity variations for the dominant frequency is  $18.5(5) \text{ km s}^{-1}$  and for the second frequency  $4.0(5) \text{ km s}^{-1}$ . Assuming the seismic radius  $R_s = 1.47R_\odot$ , we get  $|\varepsilon(A_{\text{Vrad}}, R)| = 0.0190(5)$  for  $\nu_1$  and  $|\varepsilon(A_{\text{Vrad}}, R)| = 0.0032(5)$  for  $\nu_2$ .

It is important to add that we cannot attach the above equation to the system of equations for the photometric amplitudes (Eq. 2) and derive simultaneously the parameters  $\varepsilon$  and  $f$ , because the time span between photometric and spectroscopic observations is too large. The Strömgren photometry was gathered in 1988 (Rolland et al. 1991) and the spectroscopy in 1976 (Kim et al. 1993). Thus, the phases of the light variations and radial velocity are not consistent.

Nevertheless, it still makes sense to compare the values of the intrinsic amplitudes  $\varepsilon$  derived in Sect. 3.1 with the estimate from Eq. 12.

In Fig. 8, we plot the empirical values of  $|\varepsilon|$  as obtained from our method for models depicted in Fig. 7. As before, four values of the microturbulent velocity were considered  $\xi_t = 2, 4, 8$  and  $10 \text{ km s}^{-1}$ . The top and bottom panel corresponds to the first and second frequency, respectively. The horizontal lines mark the range of  $|\varepsilon|$  estimated from the amplitude of the radial velocity derived by Kim et al. (1993). As one can see, we got the agreement of  $|\varepsilon|$  between the values from our method and the estimates from  $A_{\text{Vrad}}$  for both frequencies simultaneously if the mass is less than about  $1.15M_\odot$  and the microturbulent velocity in the atmosphere is at least  $4 \text{ km s}^{-1}$ . This result is in agreement with previous constraints derived from the parameter  $f$ . We can also tentatively say that the intrinsic amplitude of the radial fundamental mode of SX Phe is about six times the intrinsic amplitude of the radial first overtone mode.

### 3.2 The values of $f$ for models fitting the two frequencies: the effect of opacities

Now, we return to the parameter  $f$  and will make detailed comparisons of their empirical and theoretical values for seismic models described in Sect. 2. These models reproduce the two radial-mode frequencies and have the effective temperature and luminosity within the  $3\sigma$  errors of the observed values. In Fig. 9, we show such comparison for the OPAL seismic model with the chemical composition  $X_0 = 0.68$ ,  $Z = 0.002$  and the parameters:  $M = 1.06M_\odot$ ,  $\log T_{\text{eff}} = 3.8867$ ,  $\log L/L_\odot = 0.834$ ,  $R = 1.47R_\odot$ . Its rotational velocity is  $14.4 \text{ km s}^{-1}$ . The left panel corresponds to the dominant frequency  $\nu_1 = 18.193565 \text{ d}^{-1}$  and the right panel to the second frequency  $\nu_2 = 23.37928 \text{ d}^{-1}$ . As one can see, for the dominant frequency we have the agreement between the empirical and theoretical values of  $f$  if the MLT parameter is in the range  $(0.5, 1.0)$  and  $\xi_t \in (8, 10) \text{ km s}^{-1}$ . The agreement for  $\xi_t = 8 \text{ km s}^{-1}$  is marginal only if  $\alpha_{\text{MLT}} = 0.7$ . For the second frequency we could not match the empirical and theoretical values of  $f$  for any microturbulent velocity. The frequency  $\nu_2$  has the photometric amplitude about 3 times smaller than the dominant frequencies. Thus, the amplitudes and phases of  $\nu_2$  could be derived not enough precisely. Certainly, new photometric time-series observations made simultaneously with time-series spectroscopy, to include also the radial velocity into the method, could help settle this point.

For the OPAL seismic model computed with the initial hydrogen abundance  $X_0 = 0.67$  the agreement is worse and only possible for the microturbulent velocity  $\xi_t = 10 \text{ km s}^{-1}$ . However, determinations of the empirical parameter  $f$  with  $\xi_t = 10 \text{ km s}^{-1}$  have much worse goodness of the fit (2–4 times larger  $\chi^2$  in Eq. 4) than for other values of  $\xi_t$ .

In Fig. 10, we compare the empirical and theoretical values of  $f$  for the OPAL seismic model with the chemical ( $X_0 = 0.70$ ,  $Z = 0.002$  and the parameters:  $M = 1.082M_\odot$ ,  $\log T_{\text{eff}} = 3.8814$ ,  $\log L/L_\odot = 0.819$ ,  $R = 1.48R_\odot$ ). Its rotational velocity is  $23 \text{ km s}^{-1}$ . In this case, we got the solution for the empirical values of  $f$  determined with the microturbulent velocity  $\xi_t = 8 \text{ km s}^{-1}$  and the theoretical values of  $f$  computed for the mixing length parameter  $\alpha_{\text{MLT}} \in (0.0, 0.5)$ . As before, we

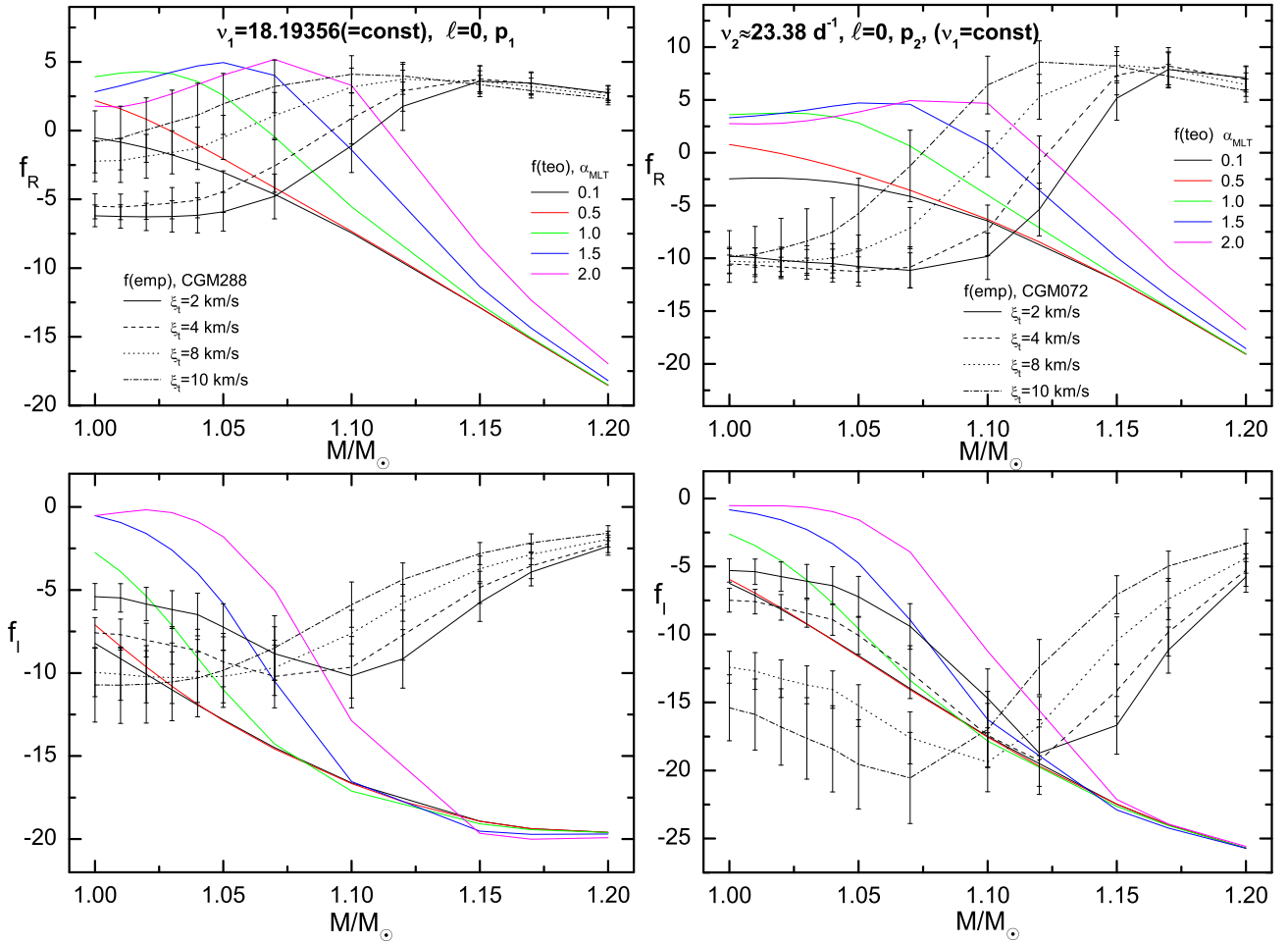


**Figure 7.** A comparison of the theoretical and empirical values of  $f$  in a function of a mass. All models fit the radial fundamental mode  $\nu_1 = 18.19356 \text{ d}^{-1}$ . The (semi)empirical values of  $f$  were determined from the Strömgren amplitudes and phases assuming the Vienna model atmospheres with different values of the microturbulent velocity  $\xi_t$ .

excluded the solution with  $\xi_t = 10 \text{ km s}^{-1}$  and  $\alpha_{\text{MLT}} = 0.7$  because of much worse fit of the photometric amplitudes and phases.

Again, for the second frequency, the empirical and theoretical values of  $f$  could not be reconciled for any value of  $\alpha_{\text{MLT}}$  and  $\xi_t$ .

The next two figures show comparisons of the theoretical and empirical values of  $f$  for seismic models found with the OP and OPLIB data; Fig. 11 and Fig. 12, respectively. Quite surprisingly, these comparisons are qualitatively similar to the comparison for the OPAL seismic models (Figs. 9 and 10), despite of significantly different masses and chemical composition. In the case of the OP seismic model, we can see that the theoretical and empirical values of  $f$  of the dominant mode agree if the mixing length parameter is in the range  $\alpha_{\text{MLT}} \in (0.0, 0.5)$  and the microturbulent velocity in the atmosphere is  $\xi_t = 8 \text{ km s}^{-1}$ . For the OPLIB seismic models, the matching for the dominant mode was possible for the range of about  $\alpha_{\text{MLT}} \in (0.5, 0.7)$  and only for  $\xi_t = 10 \text{ km s}^{-1}$ .

The first conclusion from Fig. 9–12 is that, independently of the used opacity data and despite of different parameters of models, constraints on efficiency of the outer-layer convection is very similar. Namely, convection does

not dominate the energy transport in the subphotospheric region and its efficiency is described by the mixing length parameter of about  $\alpha_{\text{MLT}} \in (0.0, 0.7)$ .

The second conclusion is that, for the range of stellar parameters considered in this work, the parameter  $f$  is not a diagnostic tool for distinguishing between seismic models calculated with different opacity data.

#### 4 SUMMARY

The goal of this paper was to construct seismic models of the star SX Phoenicis that reproduce all observables that could be extracted from the available observational data. Firstly, we made an independent mode identification from the photometric amplitudes and phases and confirmed pulsations of SX Phe in the two radial modes. Then, we search for models that fit the observed frequencies of the two radial modes adopting the three commonly used opacity data for evolutionary computations. The aim was to obtain models with the effective temperature and luminosity within the adopted observed errors. Besides, the requirement of instability of both pulsational modes must always be met.

The first result was that only with the OPAL data

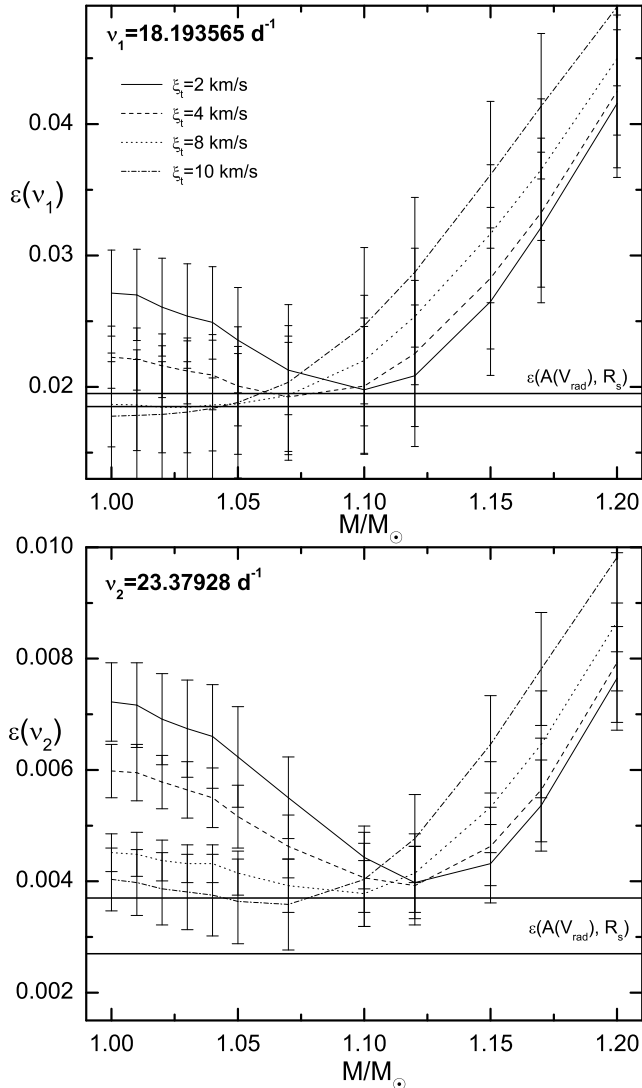


**Figure 8.** The empirical values of the intrinsic mode amplitude  $|\varepsilon|$  for models considered in Fig. 7. The top panel correspond to the dominant frequency (the radial fundamental mode) and the bottom panel to the second frequency (the first radial overtone). The horizontal lines mark the range of  $|\varepsilon(A(V_{\text{rad}}), R_s)|$  estimated from the radial velocity amplitudes and assuming the seismic radius  $R_s = 1.47R_\odot$ .

it was possible to construct such seismic models having a typical chemical composition for this prototype. Our best seismic OPAL models have the initial hydrogen abundance in the range  $X_0 \in (0.67, 0.70)$  and metallicity  $Z = 0.002$ . Their masses are of about  $M = 1.05 - 1.08 M_\odot$ , the radii:  $R = 1.47 - 1.48 R_\odot$  and the age: 2.80 – 3.07 Gyr. All seismic models are in the post-main sequence phase and burn hydrogen in the shell. The best seismic model of SX Phe found by Petersen & Christensen-Dalsgaard (1996) with the old OPAL opacities (Iglesias et al. 1992) had a mass  $M = 1.0 M_\odot$ , metallicity  $Z = 0.001$ , initial hydrogen abundance  $X_0 = 0.70$  and the age 4.07 Gyr. Thus, it was much older than our best OPAL seismic models.

Then we searched for seismic models using OP and OPLIB opacity data. It appeared that in these cases, only models computed for significantly higher abundances of the

initial hydrogen and metallicity are able to account for the two radial mode frequencies and have luminosity within the  $3\sigma$  error. The OP seismic model have a mass  $M = 1.24 M_\odot$ , radius  $R = 1.55 R_\odot$  and the chemical composition  $X_0 = 0.75$ ,  $Z = 0.0034$ . It is after an overall contraction, in the hydrogen shell-burning phase, and its age is 2.62 Gyr. The OPLIB seismic model has similar parameters, namely:  $M = 1.28 M_\odot$ ,  $R = 1.56 R_\odot$ ,  $X_0 = 0.75$ ,  $Z = 0.0041$ . The model has just finished the overall contraction phase and its age is 2.31 Gyr. However, we consider the OP and OPLIB seismic models as less reliable because of their high initial hydrogen abundance ( $X_0 = 0.75$ ) and metallicity ( $Z = 0.0034 - 0.0041$ ). Firstly, if SX Phoenicis would be a blue straggler, then it should have rather enhanced helium abundance (e.g., McNamara 2011; Nemec et al. 2017), hence lower hydrogen abundance. Secondly, the metallicity of the OP and OPLIB seismic models is higher than usually assumed for Population II stars. However, we currently do not have firm observables to rule out these models for certain.

In the next step, we used another seismic tool, that is the empirical values of the parameters  $\varepsilon$  and  $f$  derived from multicolour photometry. A comparison of the theoretical and empirical values of  $f$  for the dominant mode indicated low to moderately efficient convection, described by the mixing length parameter  $\alpha_{\text{MLT}} \in (0.0, 0.7)$ . This conclusion is independent of the used opacity data, that is the same values of  $\alpha_{\text{MLT}}$  were estimated for seismic models computed with the OPAL, OP and OPLIB tables. Moreover, this analysis showed that the microturbulent velocity in the atmosphere amounts to about  $\xi_t \in (4, 8) \text{ km s}^{-1}$ . Thus, despite a low mass of SX Phe ( $M \approx 1.06 - 1.08 M_\odot$  for the OPAL seismic models), convective transport in its outer layers is not very efficient. This is because the radiative gradient is significantly reduced due to much lower opacity caused by very low metallicity.

The intrinsic mode amplitude,  $\varepsilon$ , of both frequencies derived from multicolour photometry are consistent with the values obtained from the radial velocity amplitudes. The relative radius variation for the radial fundamental mode is about 2 per cent and for the first overtone about 0.3 per cent.

Such comprehensive seismic studies of pulsators like SX Phoenicis are very important for deriving constraints on convection in the outer layers, because the star is on the border between very efficient and inefficient convection. More stringent constraints from our complex seismic modelling could be derived for pulsators in double-lined eclipsing binaries. We plan to make such studies in the near future.

## ACKNOWLEDGEMENTS

The work was financially supported by the Polish NCN grant 2018/29/B/ST9/02803.

## DATA AVAILABILITY

Data on the photometric amplitudes and phases underlying this article are available in Rolland et al. (1991). Our theoretical computations will be shared on reasonable request to the corresponding author.

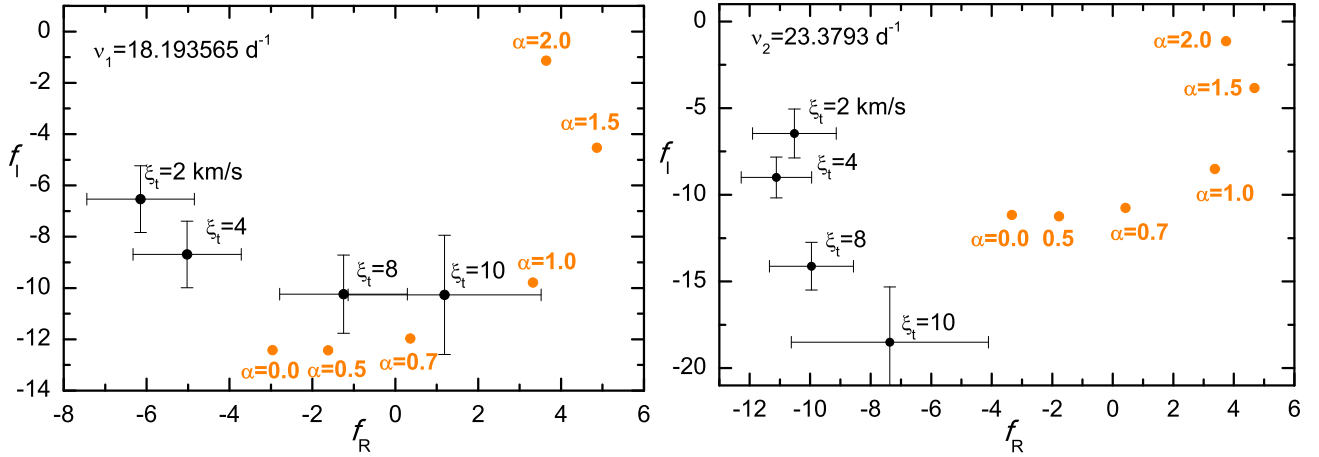


**Figure 9.** A comparison of the theoretical and empirical values of  $f$  on the complex plane for the radial fundamental mode (the left panel) and for the first overtone mode (the right panel). The theoretical values were computed for the OPAL seismic model with parameters:  $X_0 = 0.68$ ,  $Z = 0.002$ ,  $M = 1.06 M_\odot$ ,  $\log T_{\text{eff}} = 3.8867$ ,  $\log L/L_\odot = 0.834$ ,  $R = 1.47 R_\odot$ , that rotates with the velocity of about  $14 \text{ km s}^{-1}$ . The model is marked with a dot on the cyan evolutionary track in Fig. 3. Different values of the mixing length parameter  $\alpha_{\text{MLT}}$  were considered. The (semi)empirical counterparts were determined from the Strömgren photometry and the Vienna model atmospheres assuming different values of the microturbulent velocity  $\xi_t$ .

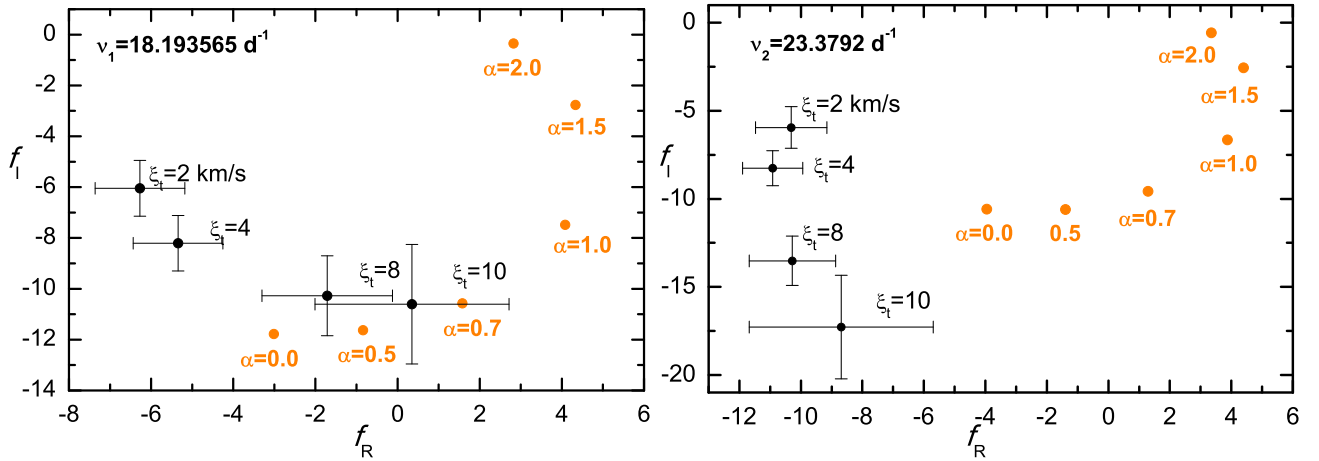


**Figure 10.** The same comparison as in Fig. 9 but for the seismic OPAL model with parameters:  $X_0 = 0.70$ ,  $Z = 0.002$ ,  $M = 1.082 M_\odot$ ,  $\log T_{\text{eff}} = 3.8814$ , and  $\log L/L_\odot = 0.819$  (within the  $3\sigma$  error), rotating with the velocity of  $23.6 \text{ km s}^{-1}$ . The model is marked with a dot on the green evolutionary track in Fig. 3.

## REFERENCES

- Andreasen G. K., 1983, *A&A*, 121, 250  
 Antoci V., Cunha M. S., Bowman D. M., et al. 2019, *MNRAS*, 490, 4040  
 Asplund M., Grevesse N., Sauval A. J., Scott P., 2009, *Annu.Rev.Astron.Astrophys.*, 47, 481  
 Canuto V. M., Goldman I., Mazzitelli I., 1996, *ApJ*, 473, 550  
 Claret A., 2000, *A&A*, 363, 1081  
 Coates D. W., Dale M., Halprin L., et al. 1979, *MNRAS*, 187, 83  
 Colgan J., Kilcrease D. P., Magee N. H., et al. 2015, *High Energy Density Physics*, 14, 33  
 Colgan J., Kilcrease D. P., Magee N. H., et al. 2016, *ApJ*, 817, 116  
 Cox A. N., King D. S., Hodson S. W., 1979, *ApJ*, 228, 870  
 Daszyńska-Daszkiewicz J., 2007, *Comm. in Asteroseismology*, 150, 32  
 Daszyńska-Daszkiewicz J., Dziembowski W. A., Pamyatnykh A. A., Goupil M.-J., 2002, *A&A*, 392, 151  
 Daszyńska-Daszkiewicz J., Dziembowski W. A., Pamyatnykh A. A., 2003, *A&A*, 407, 999  
 Daszyńska-Daszkiewicz J., Dziembowski W. A., Pamyatnykh A. A., et al. 2005a, *A&A*, 438, 653  
 Daszyńska-Daszkiewicz J., Dziembowski W. A., Pamyatnykh A. A., 2005b, *A&A*, 441, 641  
 Daszyńska-Daszkiewicz J., Pamyatnykh A. A., Walczak P., et al. 2017, *MNRAS*, 466, 2284  
 Daszyńska-Daszkiewicz J., Walczak P., Pamyatnykh A. A., et al. 2020, in *Stars and Their Variability Observed from Space*, eds. C. Neiner, W. Weiss, D. Baade et al., p. 237  
 Dziembowski W. A., 1977a, *Acta Astr.*, 27, 95  
 Dziembowski W. A., 1977b, *Acta Astr.*, 27, 203  
 Dziembowski W., Kozłowski M., 1974, *Acta Astr.*, 24, 245  
 Eggen O. J., 1952a, *PASP*, 64, 31  
 Eggen O. J., 1952b, *PASP*, 64, 305  
 Eggen O. J., Cox A. N., 1989, *AJ*, 97, 431  
 Ferguson J. W., Alexander D. R., Allard F., et al. 2005, *ApJ*, 623, 585  
 Garrido R., Rodriguez E., 1996, *MNRAS*, 281, 696

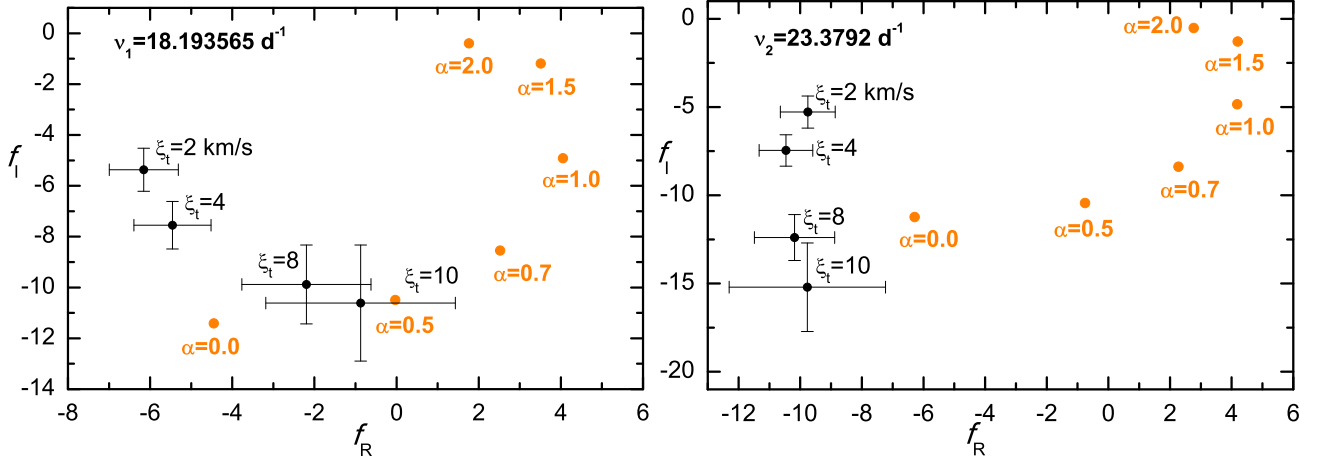


**Figure 11.** The same comparison as in Fig.9 but for the OP seismic model with parameters:  $X_0 = 0.75$ ,  $Z = 0.0034$ ,  $M = 1.24M_\odot$ ,  $\log T_{\text{eff}} = 3.8725$ , and  $\log L/L_\odot = 0.820$  (within the  $3\sigma$  error),  $R = 1.55 R_\odot$  and the rotational velocity of  $17 \text{ km s}^{-1}$ . The model is marked with a dot on the dashed evolutionary track in Fig. 3.

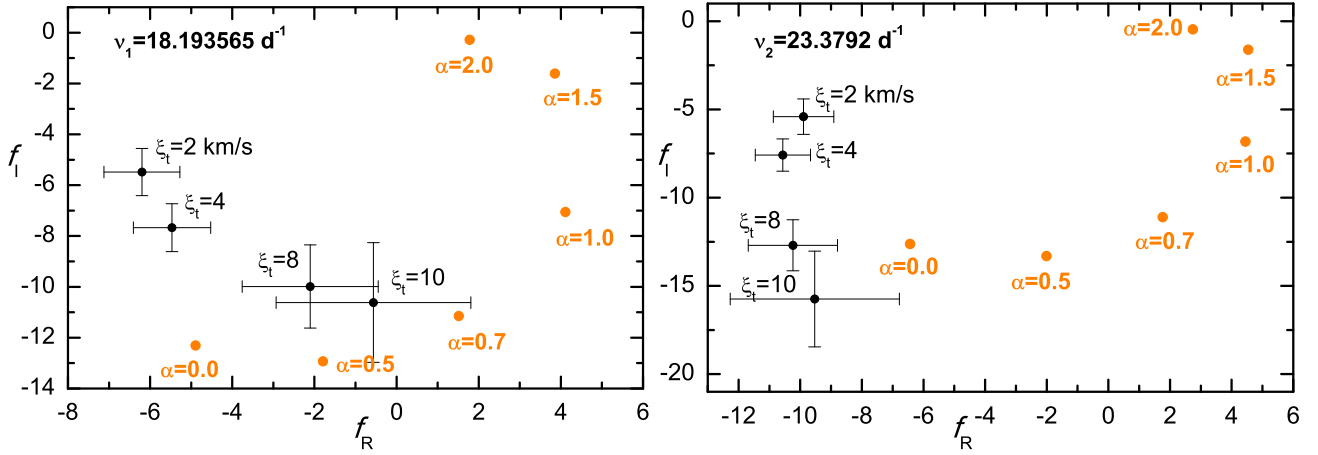


**Figure 12.** The same comparison as in Fig.9 but for the OPLIB seismic model with parameters:  $X_0 = 0.75$ ,  $Z = 0.0041$ ,  $M = 1.28M_\odot$ ,  $\log T_{\text{eff}} = 3.8763$ , and  $\log L/L_\odot = 0.845$ ,  $R = 1.56 R_\odot$  and the rotational velocity of  $5.5 \text{ km s}^{-1}$ . The model is marked with a dot on the dotted evolutionary track in Fig. 3.

Heiter U., Kupka F., van't Veer-Menneret C., et al. 2002, A&A, 392, 619  
 Hubeny I., Lanz T., 2011, Synspec: General Spectrum Synthesis Program (ascl:1109.022)  
 Hubeny I., Lanz T., 2017, arXiv e-prints, p. [arXiv:1706.01859](https://arxiv.org/abs/1706.01859)  
 Iglesias C. A., Rogers F. J., 1996, ApJ, 464, 943  
 Iglesias C. A., Rogers F. J., Wilson B. G., 1992, ApJ, 397, 717  
 Kim C., McNamara D. H., Christensen C. G., 1993, AJ, 106, 2493  
 Kippenhahn R., Weigert A., Weiss A., 2012, Stellar Structure and Evolution. Springer-Verlag Berlin  
 Landes H., Bamberg K. R., Coates D. W., et al. 2007, PASAustral., 24, 41  
 McNamara D. H., 1997, PASP, 109, 1221  
 McNamara D. H., 2011, AJ, 142, 110  
 Nemec J. M., Balona L. A., Murphy S. J., et al. 2017, MNRAS, 466, 1290  
 Pamyatnykh A. A., 1999, Acta Astr., 49, 119  
 Pamyatnykh A. A., Dziembowski W. A., Handler G., et al. 1998, A&A, 333, 141  
 Petersen J. O., Christensen-Dalsgaard J., 1996, A&A, 312, 463  
 Rodriguez E., Lopez-Gonzales M. J., Lopez de Coca P., 2000, A&A Suppl. Ser., 144, 469

Rogers F. J., Nayfonov A., 2002, ApJ, 576, 1064  
 Rogers F. J., Swenson F. J., Iglesias C. A., 1996, ApJ, 456, 902  
 Rolland A., Rodriguez E., Lopez de Coca P., et al. 1991, A&A Suppl., 91, 347  
 Seaton M. J., 1996, MNRAS, 279, 95  
 Seaton M. J., 2005, MNRAS, 362, L1  
 Vandenberg D. A., 1985, ApJ Suppl., 58, 711  
 Walczak P., Daszyńska-Daszkiewicz J., Pigulski A., Pamyatnykh A. A., et al. 2019, MNRAS, 485, 3544

This paper has been typeset from a  $\text{\LaTeX}$  file prepared by the author.